



Rich-club reorganization and related network disruptions are associated with the symptoms and severity in classic trigeminal neuralgia patients

Pengfei Zhang^{a,b,1}, Xinyue Wan^{c,1}, Kai Ai^d, Weihao Zheng^e, Guangyao Liu^{a,b}, Jun Wang^{a,b}, Wenjing Huang^{a,b}, Fengxian Fan^b, Zhijun Yao^{e,*}, Jing Zhang^{b,f,*}

^a Second Clinical School, Lanzhou University, Lanzhou 730000, China

^b Department of Magnetic Resonance, Lanzhou University Second Hospital, Lanzhou 730000, China

^c Department of Radiology, Huashan Hospital, Fudan University, Shanghai 200040, China

^d Philips, Healthcare, Xi'an 710000, China

^e Gansu Provincial Key Laboratory of Wearable Computing, School of Information Science and Engineering, Lanzhou University, Lanzhou 730000, China

^f Gansu Province Clinical Research Center for Functional and Molecular Imaging, Lanzhou 730030, China

ARTICLE INFO

Keywords:

Trigeminal neuralgia
Chronic pain
Structural network
Functional network
Graph theory analysis
Rich-club organization

ABSTRACT

Background: Alterations in white matter microstructure and functional activity have been demonstrated to be involved in the central nervous system mechanism of classic trigeminal neuralgia (CTN). However, the rich-club organization and related topological alterations in the CTN brain networks remain unclear.

Methods: We simultaneously collected diffusion-tensor imaging (DTI) and resting state functional magnetic resonance imaging (rs-fMRI) data from 29 patients with CTN (9 males, mean age = 54.59 years) and 34 matched healthy controls (HCs) (12 males, mean age = 54.97 years) to construct structural networks (SNs) and functional networks (FNs). Rich-club organization was determined separately based on each group's SN and different kinds of connections. For both network types, we calculated the basic connectivity properties (network density and strength) and topological properties (global/local/nodal efficiency and small worldness). Moreover, SN-FN coupling was obtained. The relationships between all those properties and clinical measures were evaluated.

Results: Compared to their FN, the SN of CTN patients was disrupted more severely, including its topological properties (reduced network efficiency and small-worldness), and a decrease in network density and strength was observed. Patients showed reorganization of the rich-club architecture, wherein the nodes with decreased nodal efficiency in the SN were mainly non-hub regions, and the local connections were closely related to altered global efficiency and whole brain coupling. While the cortical-subcortical connections of feeder were found to be strengthened in the SN of patients, the coupling between networks increased in all types of connections. Finally, disease severity (duration, pain intensity, and affective alterations) was negatively correlated with coupling (rich-club, feeder, and whole brain) and network strength (the rich-club of the SN and local connections of the FN). A positive correlation was only found between pain intensity and the coupling of local connections.

Conclusions: The SN of patients with CTN may be more vulnerable. Accompanied by the reorganization of the rich-club, the less efficient network communication and the impaired functional dynamics were largely attributable to the dysfunction of non-hub regions. As compensation, the pain transmission pathway of feeder connections involving in pain processing and emotional regulation may strengthen. The local and feeder sub-networks may serve as potential biomarkers for diagnosis or prognosis.

* Corresponding authors at: Gansu Provincial Key Laboratory of Wearable Computing, School of Information Science and Engineering, Lanzhou University, No. 222 South Tianshui Road, Lanzhou 730000, China (Z. Yao). Department of Magnetic Resonance, Lanzhou University Second Hospital, Cuiyingmen No.82, Chengguan District, Lanzhou 730030, China (J. Zhang).

E-mail addresses: yaozj@lzu.edu.cn (Z. Yao), ery_zhangjing@lzu.edu.cn (J. Zhang).

¹ These authors contributed equally to this study.

<https://doi.org/10.1016/j.nicl.2022.103160>

Received 24 March 2022; Received in revised form 20 July 2022; Accepted 18 August 2022

Available online 23 August 2022

2213-1582/© 2022 The Authors. Published by Elsevier Inc. This is an open access article under the CC BY-NC-ND license (<http://creativecommons.org/licenses/by-nc-nd/4.0/>).

1. Introduction

Trigeminal neuralgia (TN) is a neuralgia disorder, with a worldwide lifetime prevalence of 0.16%–0.30% (Mueller et al., 2011). The key clinical feature of TN is often described as a short-lasting electric shock or stabbing pain attacks in the trigeminal region (Bendtsen et al., 2020). Classic TN (CTN), which is the most common subtype of TN and is usually attributable to the nerve vessel conflict (NVC) of the trigeminal nerve root (Headache Classification Committee, 2018). In addition to the NVC mechanism, a plasticity and sensitization process has been demonstrated in the central nervous system after peripheral trigeminal nerve injury (Davis et al., 2011; DeSouza et al., 2014; Taylor et al., 2009), which may widely activate intra-cerebral networks and form pathologic algogenic systems (Sabalys et al., 2013). Therefore, it is necessary to explore this central mechanism to understand the CTN pathophysiology better.

A graphic theoretical analysis allows researchers to model the information interactions between brain regions with a set of nodes and edges (Bullmore and Sporns, 2009). Previous studies that have applied graphic theoretical analysis to resting state functional magnetic resonance imaging (rs-fMRI) and diffusion-tensor imaging (DTI) data from patients with TN indicate they have a decreased functional participation coefficient and white matter network efficiency (Tsai et al., 2019; Wu et al., 2020). It has been suggested that the inefficiency of structural network (SN) and reorganization across functional networks (FNs) may be related to the modulation of continuous pain signals and the plasticity of the brain in response to chronic pain (Porcaro et al., 2020). Given that brain structural connections may be the foundation of functional execution, SN-FN coupling analysis has been proposed to combine the study of structural and functional connections (i.e., connectomics) (Baum et al., 2020; Cao et al., 2020). Decoupling has been reported in migraine patients, which indicates dynamic brain function in response to frequent headaches (Li et al., 2017). Actually, our previous study suggested there was impaired flexibility in the functional state transition of CTN patients (Zhang et al., 2021). Hence, the simultaneous investigation of SN and FN, and their coupling relationship in CTN patients may provide further supplementary evidence.

In graph theory, the rich-club plays a critical role in brain topological organization, due to its high inter-connection and the central hub regions within it (Hagmann et al., 2008; van den Heuvel et al., 2012; van den Heuvel and Sporns, 2011). Accumulating evidence indicates that a rich-club efficiently contributes to global communication, as well as to the flexibility and plastic nature of brain networks (Crossley et al., 2013; Misić et al., 2016). Several investigations of fibromyalgia and migraine that have focused on rich-club organization suggest it involves reorganization of hub regions, implying the loss of optimal topological organization in chronic pain conditions (Kaplan et al., 2019; Li et al., 2017; Liu et al., 2015). Recently, various brain regions, such as the thalamus, the striatum, the cingulate cortex, the frontal, insular, and the somatosensory cortex, have been identified as being involved in central plasticity in CTN because of their alterations of function and the fibers passing through them (DeSouza et al., 2014; Henssen et al., 2019b; Tsai et al., 2018; Wang et al., 2017; Wu et al., 2020). However, the specific roles of these regions in the topological hierarchy of CTN and their possible reorganization remain unknown.

In this study, we hypothesized that CTN patients exhibit reorganization of rich-club regions, which could be related with the disproportional disruption of SN and FN topology, as well as the coupling between networks.

2. Methods

2.1. Participants and clinical assessments

We recruited 38 patients with CTN from Lanzhou University Second Hospital, and 41 healthy controls (HCs) matched for age, sex, and

education. Two experienced neurologists made the diagnosis based on the International Classification of Headache Disorders (ICDH-III) (Headache Classification Committee, 2018), and NVC was confirmed by an MRI or surgery. All patients complained they experienced pain for >1 year, without obvious sensory deficits. Lesions leading to secondary TN were excluded by high-resolution imaging around the trigeminal nerve. The other exclusion criteria were: (1) microvascular decompression (MVD) or any other surgical history; (2) a head trauma history; (3) other pain or neuropsychiatric conditions; (4) contraindications; (5) severe white matter hyperintensity (WMH) (Fazekas grade 3) (Wang et al., 2017); (6) being left handed; or (7) alcohol or drug addiction. The exclusion criteria of HCs were identical to CTN patients. All CTN patients received medications, which were uncontrolled during the experiment. The details about treatment are listed in Table 1. We used a visual analogue scale (VAS) ranging from 0 (no pain) to 10 (worst imaginable pain) to record pain intensity in the last 7 days; then, the average weekly score was obtained. A self-rating depression scale (SDS) and a self-rating anxiety scale (SAS) were used to evaluate the mental state of patients and HCs. The Ethics Committee of Lanzhou University Second Hospital approved the research. Based on the Declaration of Helsinki, details about the research were given to all patients, who provided written consent to participate.

2.2. Imaging acquisition

Imaging data were collected on a 3.0 T MR scanner (Ingenia CX, Philips Healthcare, the Netherlands) with a 16-channel head/neck coil. All subjects were awake and kept their eyes closed during scanning, and were instructed not to think about anything. Noise and head-motion were controlled by foam padding and earplugs. The rs-fMRI images were obtained using echo-planar imaging (EPI) (time of repetition (TR) = 2000 ms; time of echo (TE) = 30 ms; 180 volumes, field of view (FOV) = 192 × 192 mm²; matrix = 64 × 64; 36 contiguous slices with 3.4 mm slice thickness). Single shot spin echo (SE)-EPI was used for DTI data acquisition (TR = 8700 ms, TE = 90 ms, FOV = 256 × 256 mm²; matrix

Table 1
Demographic and clinical characteristics of participants.

	Patients with CTN	Healthy controls	χ^2/t value	P-value
Sex (female/male)	20/9	22/12	0.001	0.721
Age, y	54.59 ± 10.82	54.97 ± 6.78	-1.344	0.864
Education, y	11.62 ± 2.61	12.15 ± 1.88	0.825	0.357
Duration of disease, y	4.12 ± 3.25	NA	NA	NA
Attack frequency (times per day)	6.34 ± 3.51	NA	NA	NA
Score of VAS	7.93 ± 0.90	NA	NA	NA
Attack side	Right (16); Left (13)	NA	NA	NA
Medication	Carbamazepine (23)/Mecobalamin (2)/None (4)	NA	NA	NA
Surgery	MVD (17) Radiofrequency therapy (2)None (10)	NA	NA	NA
SDS	50.45 ± 10.46	32.15 ± 4.37	-9.307	<0.001
SAS	46.59 ± 6.59	32.06 ± 3.39	-11.233	<0.001

Values were displayed as mean ± standard deviation. P value of gender was calculated by chi-square test and p values of age, Education, SDS and SAS were obtained by independent-samples t test. CTN, classic trigeminal neuralgia; HC, healthy controls; VAS, visual analogue scale; SDS, self-rating depression scale; SAS, self-rating anxiety scale; MVD, microvascular decompression.

= 128 × 128, 50 slices, slice thickness = 3 mm, 64 gradient directions at b = 1000 s/mm²; and one image with b = 0). Using a sagittal Magnetization Prepared Rapid Gradient echo sequence, three-dimensional isovoxel structural images were also acquired (TR = 1900 ms; TE = 2.93 ms; FOV = 256 × 256 mm²; matrix = 256 × 256; 192 contiguous sagittal slices). The plain scan images of all the subjects were examined by an experienced radiologist to exclude any lesions or severe WMH.

2.3. DTI and fMRI preprocessing

Based on FMRIB Software Library 6.0 (FSL, <http://fsl.fmrib.ox.ac.uk/fsl/fslwiki>) (Smith et al., 2004) and the Diffusion Toolkit (DTK, <http://www.trackvis.org/dtk/>) (Wang et al., 2007), the PANDA toolbox (<http://www.nitrc.org/projects/panda>) (Cui et al., 2013) was used under the default parameters to preprocess the DTI data. The preprocessing included skull stripping, eddy current and head motion corrections, and calculation for diffusion tensor and fractional anisotropy (FA). After the normalization of the T1-weighted image and the co-registration of the FA map, the fiber paths were reconstructed using deterministic fiber tracking algorithms (Mori et al., 1999). Path tracing proceeded until two consecutive directions of movement had a crossing angle >45° or the FA was outside the range (0.2–1) (Guo et al., 2021).

The rs-fMRI data were preprocessed with the toolbox for Data Processing & Analysis of Brain Imaging (DPABI, <http://rfmri.org/dpabi>) (Chao-Gan and Yu-Feng, 2010). After discarding the first 10 volumes, the slice-timing and realignment were applied to the remaining data. Based on the head-motion evaluation, we excluded 9 CTN patients and 7 HCs (mean framewise displacement (FD) (Jenkinson) >0.2 mm or a head displacement >1.5 mm, maximum rotation >1.5°). The FD between the final participants in the two groups were not statistically different ($t = 1.425, p = 0.159$). Then, the following steps were performed: co-registration with anatomic images, normalization to Montreal Neurological Institute (MNI) space, detrending, regressing nuisance variables (head-motion parameters, white matter, cerebrospinal fluid, and global signal), and bandpass filtering (0.01–0.1 Hz). As suggested in a previous study, smoothing was not performed to avoid artificial local spatial correlations (Wang et al., 2009).

2.4. Network construction

The nodes of the SN and FN were determined using the Brainnetome

(BN) Atlas (Fan et al., 2016), which divides the whole brain into 210 cortical and 36 subcortical regions (Fig. 1A). For the SN construction, the connection density, which reveals the number of connections per unit surface and has been applied in previous studies (Gong et al., 2009; Guo et al., 2021; Zhang et al., 2011), was calculated as the weight of the edges (Honey et al., 2009) (Supplementary method). To exclude spurious edges, the connections with fiber numbers (FN) lower than 3 were removed. Regarding the FN, Pearson’s correlation coefficient (r) with a Fisher z transformation was computed as the connection strength between nodes. The negative edges were reserved by calculating their absolute values.

Subsequently, a 246 × 246 symmetric and weighted SN and FN were used to calculate the connectivity properties of network and the SN-FN coupling coefficient. For rich-club and graph theoretical analysis, undirected and binarized matrices were generated by retaining the positive edges in the SN and the edges in the FN that exceeded the threshold of $p < 0.05/30135$ (Bonferroni corrected).

2.5. Rich-club organization of the SN

The detailed methods about rich-club detection have been described in previous studies (van den Heuvel et al., 2012; van den Heuvel and Sporns, 2011). Based on the binarized SN, the rich-club in both groups were explored by calculating the normalized rich-club coefficient $\Phi_{norm}^w(k)$, which was defined as the ratio of $\Phi^w(k)$ and $\Phi_{random}^w(k)$. The rich-club coefficient $\Phi^w(k)$ was obtained according to the formula:

$$\Phi^w(k) = \frac{2W_{>k}}{N_{>k}(N_{>k} - 1)}$$

where k is the number of edges attached to a node; $N_{>k}$ represented the quantity of nodes with a degree larger than k ; and $W_{>k}$ reflected the actual connections between the remaining nodes. The $\Phi_{random}^w(k)$ was the mean value of the $\Phi^w(k)$ from a set of 1,000 random networks with a similar nodal distribution and degree density. A rich-club regime was considered to exist, when the $\Phi_{norm}^w(k) > 1$.

In order to identify the rich-club regions of each group, the edges present in at least 75% of subjects were selected to comprise, respectively, the average SN of the CTN and HC groups (Kaplan et al., 2019; Shu et al., 2018). According to the rank of the nodal degree, the top 10% nodes with the highest degree were defined as rich-club regions (Peng et al., 2021; van den Heuvel et al., 2013). The spatial distribution of rich-

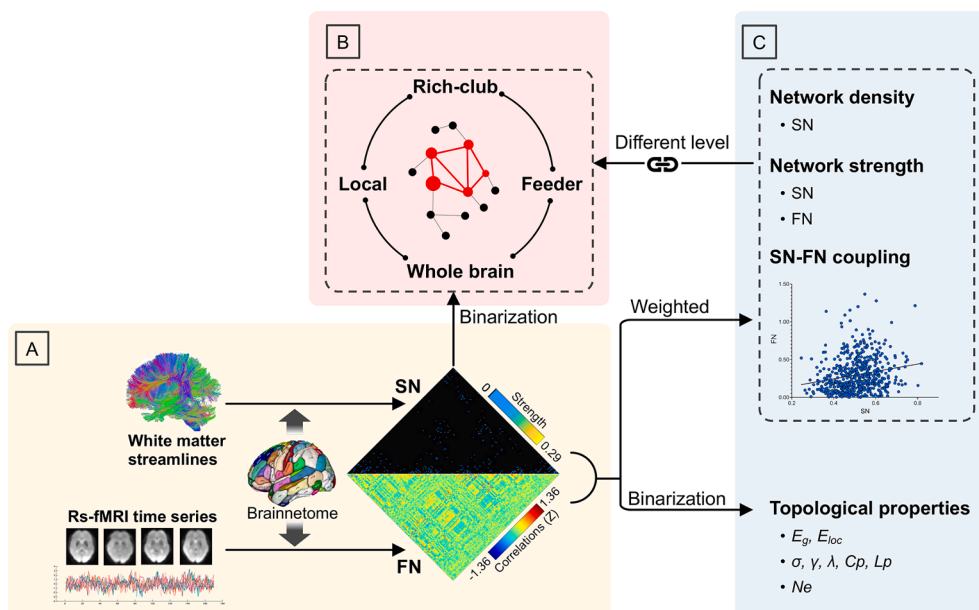


Fig. 1. The flowchart of analytical process. (A) Based on the parcellation of the Brainnetome Atlas, the rs-fMRI and DTI data was used to construct the FN and SN, respectively. The matrix displayed in figure came from one of CTN patients. (B) After binarizing the SN, network hierarchy was identified and hub regions were selected for the CTN and HC groups, separately. All the connections were divided into four types: whole brain, rich-club, feeder, and local connections. (C) Both global and nodal topological properties were calculated in the binarized FN and SN. The weighted networks were used for calculating network density, strength and the coupling relationships between FN and SN, and all the metrics were investigated in different connectivity levels. SN, structural network; FN, functional network; rs-fMRI, resting state functional magnetic resonance imaging.

club regions was displayed with Brainnet viewer (<https://www.nitrc.org/projects/bnv/>) (Xia et al., 2013). Subsequently, the connections of all the matrices were categorized into three types of edges (van den Heuvel et al., 2012): (I) rich-club connections – those connecting rich-club regions to each other; (II) feeder connections – those connecting rich-club regions to non-rich-club regions; and (III) local connections – those connecting non-rich-club regions to each other (Fig. 1B).

2.6. Topological analysis

The basic topological measurements included connectivity strength (the sum of the weights in the matrices) and connectivity density (the ratio of actual edge numbers over the total possible edges). Due to the sparsity of the SN, the connectivity density was only calculated for the SN. All those connectivity properties were evaluated at the whole brain level and different kinds of sub-networks, as well. Moreover, other global metrics (global efficiency (E_g), local efficiency (E_{loc}), small-worldness (σ), normalized clustering coefficient (γ), normalized characteristic path length (λ), clustering coefficient (C) and shortest path length (L)) and regional graph metrics (nodal efficiency (E_{nodal})) were calculated using the GRETNA toolbox (www.nitrc.org/projects/gretna) (Hagmann et al., 2008; Rubinov and Sporns, 2010; Wang et al., 2015) (Fig. 1C).

2.7. SN-FN coupling analysis

Correlation between the FN and SN were performed to evaluate the relationship between the functional connectomics and the underlying anatomic connections. By using the method recommended in previous studies, the nonzero edges in the SN were extracted and rescaled into a Gaussian distribution (Hagmann et al., 2010; Honey et al., 2009). Then, these selected connections were correlated with their matching FN counterparts by calculating Pearson's correlation (Zhang et al., 2011). Therefore, a single coupling metric was obtained for each subject (Fig. 1C). We further repeated the coupling analysis for the whole brain and all kinds of subnetworks.

2.8. Statistical and validation analysis

Two independent samples *t*-tests were applied to detect group-differences in age, education, and head motion, while the chi-square test was used to assess gender differences between groups. Then, we performed exploratory analyses with respect to rich-club regions topological properties and coupling values. Nonparametric permutation tests (10,000 repetition) were used for rich-club coefficients, global graph metrics, connectivity properties, and SN-FN coupling, with age, sex, education, and head motion (i.e., FD Jenkinson) as covariates. Because the comparison of Φ_{norm}^w was performed over the rich-club range, a Bonferroni correction was used. Moreover, between-group comparisons of the E_{nodal} and edge strength, were performed with independent samples *t*-tests, regressing out age, sex, education, and head motion using the GRETNA toolbox, wherein the FDR correction ($p = 0.05$, 246 corrections) was applied for E_{nodal} , and the Network Based Statistic (NBS) (Zalesky et al., 2010) ($p_{link} = 0.05$, $p_{component} = 0.05$, 10,000 permutations) for edges. The relationships between the connectivity properties of different subnetworks and E_g , and also coupling strength, were assessed with Spearman's correlation; z-tests were used for the subsequent between-groups comparisons of the correlations. Spearman's partial correlations, controlling for age, sex, education, and head motion were performed between graph metrics, rich-club organization, SN-FN coupling, and clinical variables to investigate their potential relationships. The same analyses were conducted for rich-club nodes, defined as the top 8% and 12% highest degree nodes, which yielded similar results (see Supplementary material, Figs. S3–S6).

3. Results

3.1. Rich-club organization

The group-averaged rich-club coefficient (including $\Phi^w(k)$ and $\Phi_{norm}^w(k)$) of the CTN and HC groups are displayed in Fig. 2A. For both groups, the rich-club region where the $\Phi_{norm}^w(k)$ was >1 was observed between $k = 2$ and $k = 8$, which was indicative of a rich-club property in each group (van den Heuvel et al., 2013). Patients showed an increased rich-club organization at $k = 2$ ($p_{adj} < 0.05$, 10,000 permutation test with a Bonferroni correction), suggesting a higher level of connectivity between hub regions in the CTN group.

3.2. Rich-club regions in the SN

Rich-club regions were defined as the top 10% brain regions with the highest degree of group-averaged SN, for each group separately (Fig. 2B ~ D). The rich-club regions in the CTN group included the bilateral inferior parietal lobule (IPL), basal ganglia (BG), thalamus and the right medioventral occipital cortex (MVOcC), lateral occipital cortex (LOcC), postcentral gyrus (PoG), middle frontal gyrus (MFG) and the left fusiform gyrus (FuG). The distribution of hub nodes in the HCs was similar in subcortical regions, but there were different nodes in cortical regions. The rich-club regions in HCs included the bilateral BG and thalamus, and the right IPL, MVOcC, MFG, inferior temporal gyrus (ITG), posterior superior temporal sulcus (Psts) and the left FuG, superior frontal gyrus (SFG), and orbital gyrus (OrG). Details about all the rich-club regions can be found in the supplementary materials (Tables S2, S3). According to the Yeo Atlas (7 networks) (Yeo et al., 2011), subregions of the BN were assigned to the visual network (VIS), default mode network (DMN), sensorimotor network (SMN), dorsal attention network (DAN), ventral attention network (VAN), frontal parietal network (FPN), and limbic network (LIM). Additionally, subcortical regions were allocated to the subcortical network (SC). In particular, the right IPL and left PoG belonging to the SMN were rich-club members of the CTN group, but not the HC group. Conversely, the rich-club regions of the SC were reduced in patients, compared to the HCs (Fig. 2B ~ D).

3.3. The topological properties of the SN and FN

The E_g and E_{loc} of the SN were decreased in patients, as compared with HC ($p_{Eg} = 0.003$ and $p_{Eloc} = 0.007$, 10,000 permutation test). The SN in both groups demonstrated small-worldness ($\sigma > 1$); however, patients showed significantly decreased levels of small-worldness coupled with lower C , as well as a higher λ and L ($p_\sigma = 0.042$, $p_\lambda = 0.010$, $p_C = 0.010$, $p_L = 0.010$, 10,000 permutation test). No statistically significant between-group difference was observed for γ ($p_\gamma = 0.294$, 10,000 permutation test) (Fig. S1A). With respect to the FN (Fig. S1B), both groups exhibited small-worldness. However, no statistical difference was detected for any properties ($p_{Eg} = 0.056$, $p_{Eloc} = 0.072$, $p_\sigma = 0.447$, $p_\gamma = 0.475$, $p_\lambda = 0.070$, $p_C = 0.077$, $p_L = 0.060$, 10,000 permutation test).

Besides the altered global properties, nodes with reduced E_{nodal} in patients were further identified in the SN ($p < 0.05$, FDR corrected) (Fig. 3). The regions included the right MFG, which was a rich-club hub, while the rest contained both non-rich-club nodes, including the bilateral MFG, OrG, superior temporal gyrus (STG), middle temporal gyrus (MTG), MVOcC; the right SFG, inferior frontal gyrus (IFG), inferior temporal gyrus (ITG), superior parietal lobe (SPL), IPL, precuneus (PCun), PoG, cingulate gyrus (CG), lateral occipital cortex (LOcC), and the left ventromedial putamen. As indicated in the Yeo Atlas (Yeo et al., 2011) (7 networks), the regions with disrupted efficiency mainly involved cognitive control networks (the DMN, FPN, DAN, VAN, and LIM) and sensory related networks (the SMN and VIS). Details about the regions with aberrant E_{nodal} can be found in the supplementary materials (Table S3).

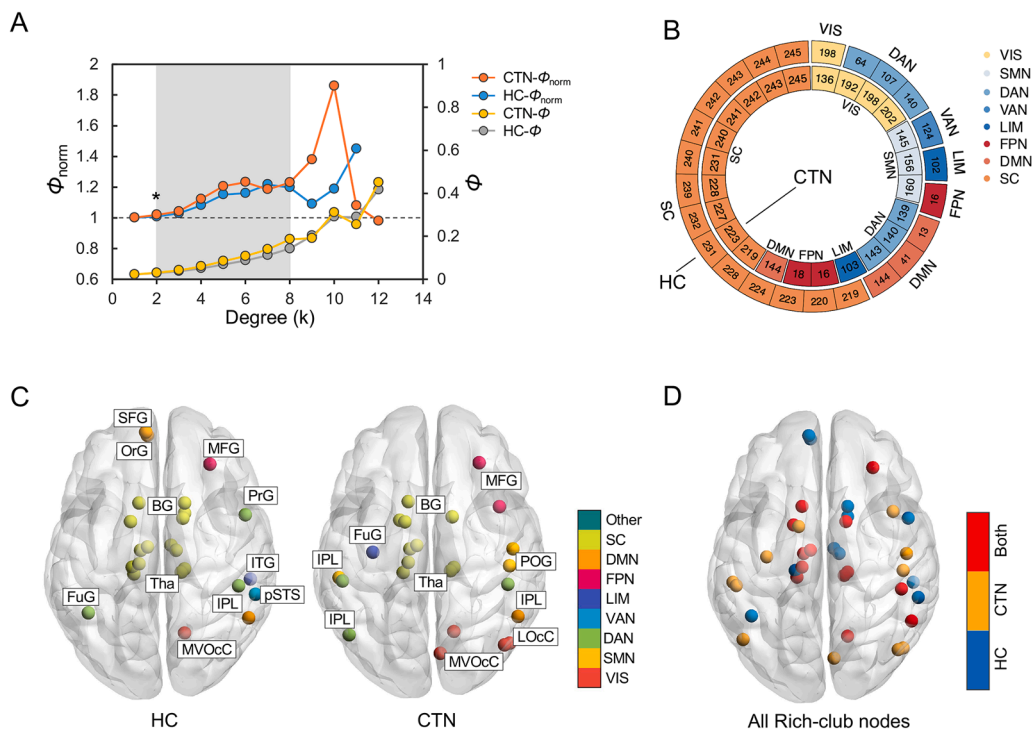


Fig. 2. Rich-club organization and hub regions for each group. (A) The rich-club coefficients (refer to the left y axis) and according normalized value (refer to the right y axis) under a series of k levels for the CTN and HC groups. Grey region highlights the range of k where the normalized coefficient > 1. Asterisk (*) represents the between group difference of normalized coefficient ($p < 0.05/7$, 10,000 permutation test with Bonferroni correction). (B) The rich-club members assigned into 8 networks based on the Yeo Atlas are displayed for each group. (C and D) The spatial maps of rich-club nodes, where nodes in figure C are colored based on different networks, but in figure D, the nodes belonging to both groups are plotted with red, and those only belonging to the CTN and HC groups are plotted with yellow and blue separately. CTN, classic trigeminal neuralgia; HC, healthy controls; MFG, middle frontal gyrus; SFG, superior frontal gyrus; FuG, fusiform gyrus; IPL, inferior parietal lobule; OrG, orbital gyrus; PrG, precentral gyrus; PoG, postcentral gyrus; ITG, inferior temporal gyrus; MVOcC, medioventral occipital cortex; LOcC, lateral occipital cortex; BG, basal ganglia, Tha, thalamus; VIS, visual network; DMN, default mode network; SMN, sensorimotor network; DAN, dorsal attention network; VAN, ventral attention network; FPN, frontal parietal network; LIM, limbic network; SC, subcortical network.

SMN, sensorimotor network; DAN, dorsal attention network; VAN, ventral attention network; FPN, frontal parietal network; LIM, limbic network; SC, subcortical network.

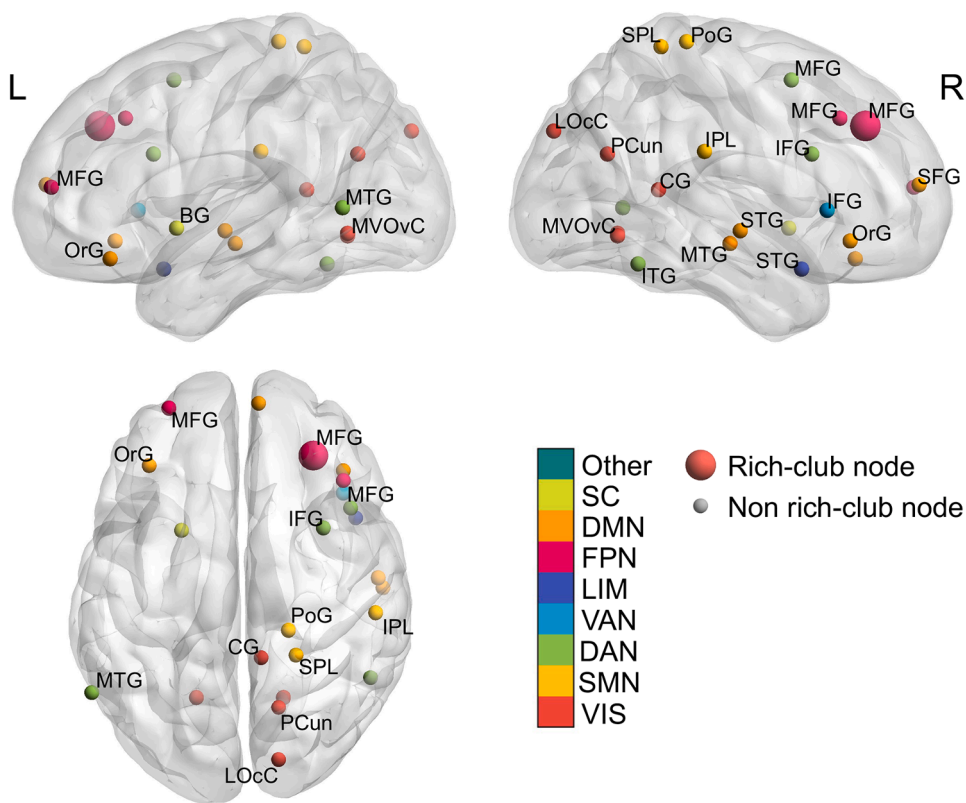


Fig. 3. Nodes with reduced efficiency in patients. The rich-club nodes and non-rich-club nodes can be distinguished by nodal size. The color of nodes represents corresponding networks. L, left; R, right; MFG, middle frontal gyrus; SFG, superior frontal gyrus; FuG, fusiform gyrus; OrG, orbital gyrus; IPL, inferior parietal lobule; SPL, superior parietal lobule; PoG, postcentral gyrus; STG, superior temporal gyrus; MTG, middle temporal gyrus; ITG, inferior temporal gyrus; MVOcC, medioventral occipital cortex; LOcC, lateral occipital cortex; PCun, precuneus; BG, basal ganglia, VIS, visual network; DMN, default mode network; SMN, sensorimotor network; DAN, dorsal attention network; VAN, ventral attention network; FPN, frontal parietal network; LIM, limbic network; SC, subcortical network.

3.4. CTN related alterations in connectivity

Based on the NBS analysis, CTN patients demonstrated enhanced structural connectivity in one component, comprising 11 nodes and 10 edges (Fig. 4). No statistical difference in functional connectivity was found. The alterations in the SN mainly involved the caudate-medial prefrontal cortex (mPFC), nucleus accumbens (NAC)-OrG, thalamus-lateral prefrontal cortex (IPFC), thalamus-precentral gyrus (PrG), thalamus-caudate (all areas were in the left hemisphere) and between the bilateral thalami. All statistical information about the altered structural edges are listed in Table S4. The altered edges were mainly feeder connections, especially in patients, as the dorsal caudate (dCa) was a hub of the patients, but not a hub of the HCs.

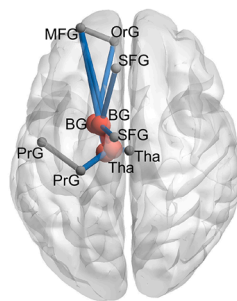
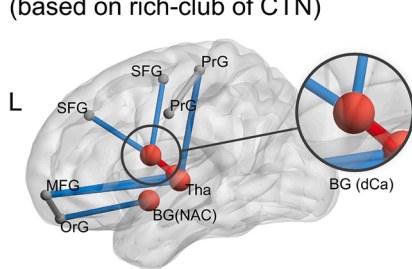
3.5. The strength and density of SN and FN

Compared with the HCs, the CTN patients showed a decreased SN density for the whole brain ($p = 0.007$), the rich-club ($p < 0.001$) and local connections ($p = 0.003$), but not feeder connections ($p = 0.183$) (Fig. S2A). As for the strength of the SN in patients, we observed a decrease of rich-club connections ($p < 0.001$), as well as an increase of feeder connections ($p = 0.037$), which was consistent with the enhanced structural edges of feeders (Fig. 4). However, no statistical difference was found for the whole brain ($p = 0.099$) or local connections ($p = 0.075$) (Fig. S2B). The strength of the FN of patients was only reduced for local connections ($p = 0.021$), whereas the whole brain ($p = 0.065$), rich-club ($p = 0.309$) and feeder connections ($p = 0.188$) did not differ significantly from the HC (Fig. S2C). All p values were obtained through 10,000 permutation tests.

3.6. Altered SN-FN coupling

Compared with the HCs, the CTN patients exhibited a higher strength of SN-FN coupling for whole brain connections, as well as rich-club, feeder, and local connections ($p_{whole\ brain} = 0.007$, $p_{rich-club} = 0.002$, $p_{feeder} = 0.001$, $p_{local} < 0.001$, 10,000 permutation tests) (Fig. 5).

A Enhanced structural connectivity in patients (based on rich-club of CTN)



B Enhanced structural connectivity in patients (based on rich-club of HC)

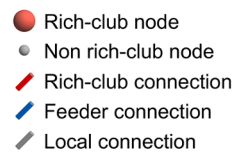
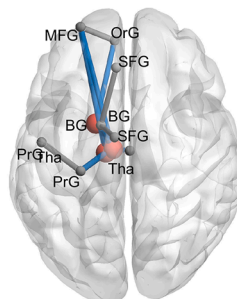
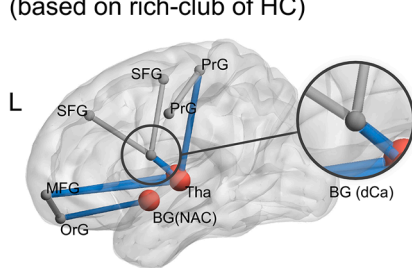


Fig. 4. Enhanced structural connections in patients. The rich-club nodes and non-rich-club nodes can be distinguished by nodal size and color. Rich-club, feeder and local connections are colored with red, blue, and grey respectively. The involved rich-club nodes were almost same in the CTN and HC groups except the dorsal caudate, which was the hub of patients and highlighted in figures. CTN, classic trigeminal neuralgia; HC, healthy controls; L, left; R, right; MFG, middle frontal gyrus; SFG, superior frontal gyrus; OrG, orbital gyrus; PrG, precentral gyrus; BG, basal ganglia; NAC, nucleus accumbens; dCa, dorsal caudate; Tha, thalamus.

3.7. Relationships between E_g of SN, coupling and different connectivity properties

In both groups, the E_g of the SN was correlated with the density of feeder and local connections in the SN, as well as the local connectivity strength of the SN (both p 's < 0.01 , Spearman correlation). The relationships between E_g -SN density of local and E_g -SN strength of local connections were stronger in the patients than the HCs (between-group difference $p < 0.01$ and $p = 0.045$, respectively, z -test). However, the correlation between E_g -SN density of rich-club in HCs ($p = 0.01$, Spearman correlation) was not found in patients ($p = 0.457$, Spearman correlation) (Fig. 6A). The whole brain coupling strength was found to be correlated with the strength of local connections in both the HC and CTN groups. While for the former, the relationship existed in the FN ($p = 0.044$, Spearman correlation), but in the SN for the later ($p = 0.033$, Spearman correlation). Details of the correlation results are presented in Table S5.

3.8. Relationship among connectivity strength, SN-FN coupling, and clinical variables

The correlations of the clinical data with the connectivity strength of the FN and SN, and the coupling strength of different kinds of connections showed that the coupling of rich-club connections was negatively correlated with disease duration (Spearman's $\rho = -0.426$, $p = 0.034$, Fig. 7A). The coupling of feeder connections showed negative correlation with both disease duration and the VAS pain score (Spearman's $\rho = -0.424$ and -0.488 respectively, with corresponding p 's of 0.035 and 0.013, Fig. 7B and C). Negative correlations also existed between the coupling of whole brain and the SDS and SAS (Spearman's $\rho = -0.412$ and -0.401 , respectively, with corresponding p 's of 0.041 and 0.047, Fig. 7E and F). The coupling of local connections was positively correlated with the VAS pain score (Spearman's $\rho = 0.478$, $p = 0.016$, Fig. 7D). We also observed a negative correlation between the VAS pain score and the SN strength of the rich-club, as well as the FN strength of local connections (Spearman's $\rho = -0.436$ and -0.419 respectively, with corresponding p 's of 0.030 and 0.037, Fig. 7G, H).

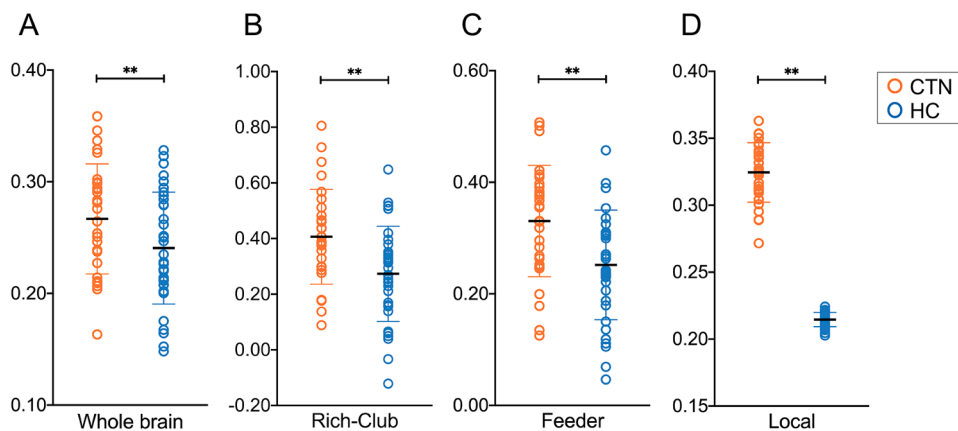


Fig. 5. SN-FN coupling. The middle black lines represent means with error bar revealing SD. Asterisk (*) represents significance of $p < 0.05$ and asterisks (**) indicate $p < 0.01$. CTN, classic trigeminal neuralgia; HC, healthy controls.

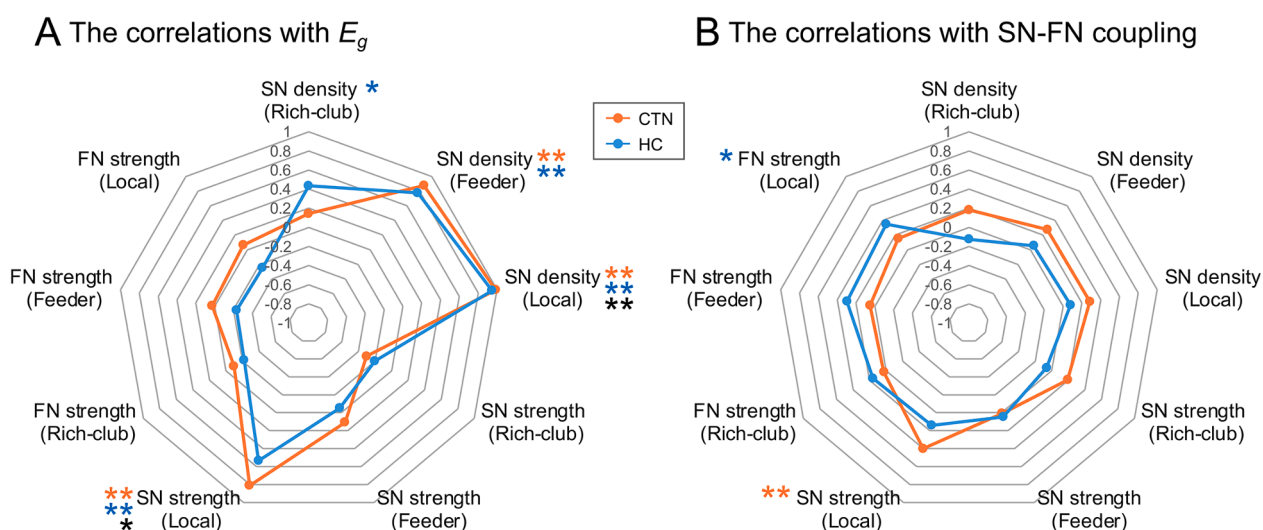


Fig. 6. The correlations of SN E_g and whole brain coupling strength with all kinds of connectivity properties. The significance of correlation results for CTN are plotted with orange asterisks, and blue for HC. Between-group differences after z-test are plotted with black asterisks. Single asterisk represents $p < 0.05$ and double ones indicate $p < 0.01$. CTN, classic trigeminal neuralgia; HC, healthy controls; SN, structural network; FN, functional network.

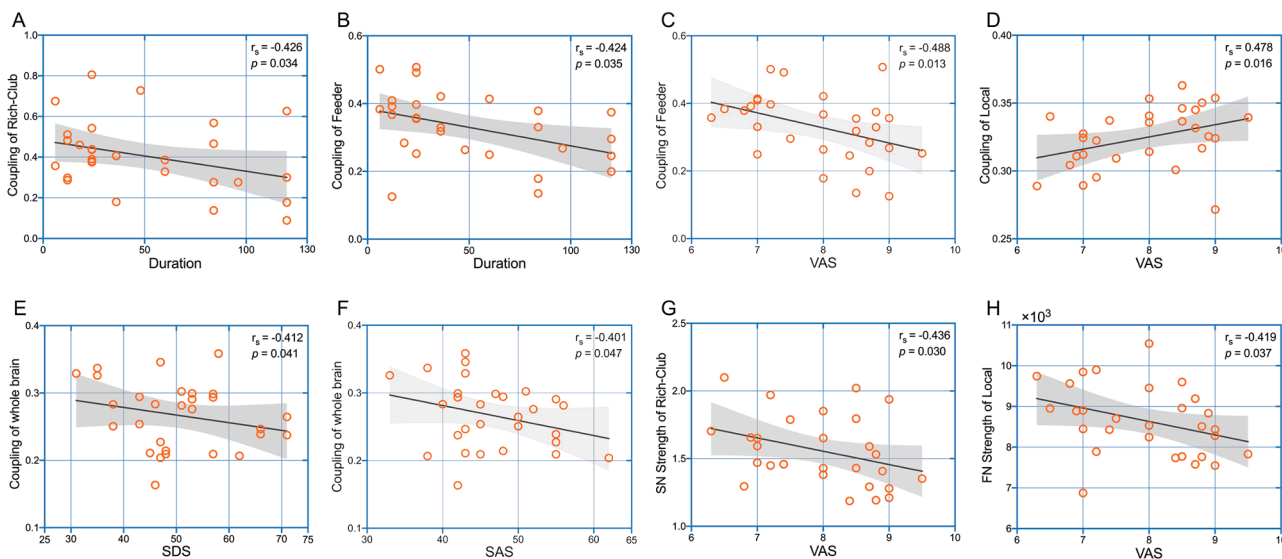


Fig. 7. The association between the clinical variables and different connectivity properties of CTN patients. VAS, visual analogue scale; SN, structural network; FN, functional network; SDS, self-rating depression scale; SAS, self-rating anxiety scale.

4. Discussion

Our simultaneous investigation of both the SN and FN in CTN patients, mainly revealed that: (1) The rich-club reorganization in CTN patients, of regions related to sensory and pain processing appeared to be new hubs, accompanied by reduced hubs in the BG; (2) Compared with HCs, patients had a broad disruption in their SN. The SN of CTN not only showed deficits in global topology, of which the reduced E_g was closely associated with the density and strength of local connections, but also exhibited decreased E_{nodal} in non-rich-club regions, along with enhanced connectivity strength in feeders, mostly involving cortical-subcortical connections; and (3) The coupling between the SN and FN was stronger in the CTN group than the HC group. In patients, the coupling of the rich-club, feeder, and the whole brain declined with the progression of disease and the deterioration of their emotional condition. However, the trends were reversed for local connections. Collectively, the present study suggests that the CTN may primarily alter the SN rather than the FN, wherein the reduced density of the local connections largely contributes to inefficient global communication and the tight relationship between networks. The enhanced feeder circuits may maintain information integration between central and peripheral areas.

4.1. Rich-club reorganization

Though a similar level of rich-club organization was found in both the CTN and HC groups, the compositions of the rich-clubs differed. Patients showed more hub regions in the SMN and less hubs in the SC. The reorganization of the rich-club in chronic pain conditions is regarded as qualitative, rather than reflecting quantitative changes in the information flow of the brain (Kaplan et al., 2019). Previous DTI studies of TN have indicated widespread disruption of global white matter microstructure, including reduced fractional anisotropy (FA) and increased mean diffusivity (MD), axial diffusivity (AD), and radial diffusivity (RD) (Tian et al., 2016; Wang et al., 2017). Those diffusion metrics may reflect the plasticity of the brain structure (Liu et al., 2018), probably related to fiber organization changes, demyelination, neuroinflammation, or edema (DeSouza et al., 2014). Though the evidence about rich-club reorganization in CTN is limited, a study of migraine, which also affects the trigeminal system (Danyluk et al., 2021), suggests that the somatosensory cortices are more densely interconnected regions in the FN (Liu et al., 2015). Consistently, the CTN specific hub in our study was mainly the postcentral gyrus, which participate in the lateral pain system, transmitting fast sharp pain signals through the lateral spinothalamic tract, and encoding pain intensity, duration, and location (Price, 2002). In addition, the appearance of new hubs compensates for or avoid the functional overload of initial hubs in the chronic stage (Stam, 2014). Hence, long-term and frequent facial attacks may consolidate the pain sensation and processing related connections for better information integration and modulation. Our findings provide further evidence from a structural perspective to support the idea that alterations in rich-club membership may be the consequence of adaptive plasticity of brain function (Liu et al., 2015).

4.2. The dysfunction of non-hub regions in the SN

Besides the reorganization of the rich-club, the inefficiency of information transfer in patients was also detected in the SN but not the FN. Further correlational analyses suggested that the aberrant efficiency was closely related with the strength and density of local connections, rather than rich-club (van den Heuvel et al., 2012; van den Heuvel and Sporns, 2011). Therefore, it was the dysfunction in the peripheral regions and local connections that contributed most to the decreased topological efficiency in our findings. Previous studies indicated that the peripheral regions were more vulnerable because of their lower level in the hierarchical network, while the central regions may be relatively resistant to the influence of disease (Cao et al., 2020; Yan et al., 2018). One recent

CTN connectomics study that focused on the white matter network also reported decreased efficiency, coupled with a dysfunction in regional information integration of the frontal, angular, and temporal gyrus, as well as the parietal and occipital cortex (Wu et al., 2020). The disruptions of E_{nodal} in our study significantly overlapped with that report, which can basically be divided into cognition related networks (the FPN, DMN, DAN, VAN, and LIM) and sensory related networks (the SMN and VIS). These regions are anatomically and widely connected through fiber tracts, such as the superior longitudinal fasciculus, fronto-occipital fasciculus, and fasciculus uncinatus, all of which have been found to be impairment in CTN patients (DeSouza et al., 2014; Liu et al., 2018). The alterations of these areas may reflect cognition-related perception and analgesia modulation (Andica et al., 2020; Iwata et al., 2005; Seminowicz et al., 2004), multisensory integration (Chiapparini et al., 2010) or the psychological complaints of chronic pain (Neudorf et al., 2020). Overall, our findings indicate that the white matter related SN was more vulnerable than the FN in CTN patients, wherein the disorders of peripheral regions involving multiple networks mainly affected global information integration.

4.3. The strengthened feeder connections in SN

Our findings indicate that strengthened structural connectivity was mainly concentrated in feeder connections, including the caudate-mPFC, NAC-OrG, and thalamus-IPFC, which explains the increased strength of the feeder in the SN. The feeder connections supply bridges between central regions and peripheral areas, through which neuronal information will usually be fed into and traverse the rich-club, and then be delivered to non-hub regions (van den Heuvel et al., 2012). The stronger connectivity may indicate the greater integration between non-hub and hub regions (Li et al., 2017). In the present study, one of the hubs in the feeder was the thalamus, a critical relay and integration center connected with the higher-order cortex (Antón-Bolaños et al., 2018; Kumar et al., 2017). The thalamus is directly involved in the trigeminal sensory pathway (Alper et al., 2021) and forms the medial pain system together with the PFC and limbic system (exactly the IPFC in the present study). As proposed, the medial system transmits slow dull pain information through the spinal reticular thalamic tract and the medial spinothalamic tract (Peyron et al., 2000), and it is linked to emotional and cognitive aspects of pain (Petrovic and Ingvar, 2002). The mPFC, OrG, and NAC have consistently been shown to be involved in emotional control (Baliki et al., 2008; Yu et al., 2014) and the reward system (May 2008). Due to abundant GABAergic neurons (Robison and Nestler, 2011) and the integration of dopaminergic and glutamatergic signals from pain related regions (such as the PFC and thalamus), the NAC is significantly involved in pain regulation and relief (Harris and Peng, 2020). A recent animal experiment suggests that optogenetic stimulation on the NAC attenuated the hyperalgesia of TN rats, accompanied by an increased extracellular concentration of GABA, glutamate, dopamine, and acetylcholine (Islam et al., 2021). Though no obvious correlation was observed between edge strength and psychological scores, which may be due to the sparsity of the SN, the aberrant links between the thalamus, NAC, and PFC may indicate an adaptive process in response to the need for emotion management in patients with chronic pain (Tu et al., 2019). The stronger connectivity related to the SMN (thalamus-PrG and caudate-mPFC) may imply an enhanced capacity to modulate pain and control jaw movement to inhibition pain (Wang et al., 2017). Taken together, considering the rich-club reorganization and the dysfunctions in peripheral regions, the strengthened feeder connections may be regarded as a compensatory mechanism, intended to produce more integration among pain processing and related emotional circuits (Hagmann et al., 2008).

4.4. The increased coupling strength

The increased SN-FN coupling in CTN patients was another main

finding. Previous studies have suggested that coupling increases with aging (Supekar et al., 2010), and in neurodegenerative and neuropsychiatric disorders (Cao et al., 2020; Dai et al., 2019; van den Heuvel et al., 2013). However, a study of migraine showed decoupling between networks in patients (Li et al., 2017). Our results, which showed increased SN-FN coupling in CTN patients, may indicate more stringent and less dynamic brain function (Hagmann et al., 2010). Consistently, our previous study of CTN, which used dynamic functional network analysis, demonstrated decreased dynamics in switching between connectivity states (Zhang et al., 2021), reflecting the inefficiency of information processing in the brain. Additionally, given the white matter impairment under the long-term nociceptive stimulation (Tian et al., 2016), the non-zero edges of the white matter network diminished further, leading to the corresponding FN limitation and closely linked to the underlying anatomical structure. It has been demonstrated that white matter integrity can predispose patients to pain chronicity, followed by the establishment of a specific FC pattern (Mansour et al., 2013). Hence, consistent with our aforementioned findings about the widespread disruptions in the SN, the significant white matter plasticity in CTN may have combined with the impaired functional dynamics to cause further differences in structural–functional coupling.

4.5. Clinical relevance

MVD has been used as the most efficacious surgical intervention for CTN, especially when symptoms do not respond to medication (Cruccu et al., 2020; Zakrzewska and Akram, 2011). Previous studies have reported that some regions, such as the insular (DeSouza et al., 2015), and hippocampus (Noorani et al., 2022), show a reverse in volume post-operatively and are valuable for predicting surgical outcomes (Danyluk et al., 2020). Besides, invasive or non-invasive stimulations of the primary motor cortex has been demonstrated to be valuable in TN modulation (Henssen et al., 2019c; Klein et al., 2015; Tsubokawa et al., 1991). However, most of the aforementioned regions were non-rich-club memberships in our study. Likewise, a study of major depressive disorder demonstrated that the feeder-local sub-network contributed to the remission of disease, rather than the rich-club (Wang et al., 2019), indicating that treatment may exert a compensatory effect by acting on non-hub areas (Kim and Min, 2020). Thus, the feeder-local connections in CTN may be provide the potential treatment targets (Henssen et al., 2019a).

Among our findings, whole brain coupling was found to be closely related with the local connections, of which the sub-network coupling positively correlated with the VAS, which was quietly the opposite for rich-club and feeder. We infer that with the progression of disease, the compensation from the rich-club and feeder coupling weakens gradually as chronic pain disproportionately affects more of the local connections, further disrupting the optimal topological organization and altering functional dynamics. The results highlight the importance of earlier and regular treatment for a shorter disease duration (Holste et al., 2020). Moreover, the altered SN-FN relationships in the present study not only spanned distinct connectivity types, but also correlated with various clinical measures, including duration, pain intensity, and abnormal emotional regulation. Therefore, the coupling may be the integrative reflection of pain and related behavioral traits, and probably captures subtle alterations in brain networks (Cao et al., 2020). Future longitudinal studies are required to investigate the impact of surgical factors on the topological hierarchy and the potential value of coupling strength as a sensitive biomarker for diagnosis or prediction.

5. Limitations

There are some limitations of the present study. First, all patients used medications for treatment before scanning. Thus, the effects of drug could not be eliminated and should be controlled in future studies (Liu et al., 2021). Moreover, though no statistically significant difference was

found in the subgroup analysis (Table S6, 7), the lateral effects of inconsistent attack side should be examined to validate our main findings in large samples. Furthermore, when calculating coupling strength, we limited the relationships within the nonzero edges of the SN. It has been suggested that a strong FC may exist between regions even when there is no direct white matter connection. More optimal metrics should be tested in future studies to reveal the indirect relationships between networks. Additionally, the limited differences in the FN between the CTN and HC groups may not only be attributable to the robustness of the network, but also to the use of relatively conventional topological properties. By using more sensitive measures, such as the hub disruption index (De Pauw et al., 2020), and combining them with machine learning methodology, more fine-grained alterations and valuable indices may be obtained.

6. Conclusion

Using multimodal and combined methods, our study revealed plastic changes in the SN and FN of CTN patients. Compared with the FN, the SN of patients was more vulnerable, manifested as rich-club reorganization and reduced efficiency in brain topology. The dysfunction of non-rich-club regions contributed mostly to a decline in global efficiency and increased coupling strength. As a compensation, the cortical-subcortical pathways related to pain processing and emotional regulation in feeder connections were strengthened. In summary, following the topological reorganization, the disproportionate interruptions of local sub-networks and the feeder compensation may provide insights into the CTN central mechanism and potential markers for diagnosis, which deserves future prospective investigations.

Funding

This work was supported by the National Natural Science Foundation of China [Grant No 81960309] and Lanzhou University Second Hospital 'Cuiying Technology Innovation Plan' Applied Basic Research Project [Grant No CY2018-MS02].

CRediT authorship contribution statement

Pengfei Zhang: Conceptualization, Data curation, Investigation, Formal analysis, Visualization, Writing – original draft. **Xinyue Wan:** Conceptualization, Data curation, Investigation, Writing – review & editing. **Kai Ai:** Conceptualization, Software, Writing – review & editing, Supervision. **Weihao Zheng:** Conceptualization, Methodology, Software, Writing – review & editing. **Guangyao Liu:** Conceptualization, Investigation, Supervision. **Jun Wang:** Data curation, Software. **Wenjing Huang:** Conceptualization, Software. **Fengxian Fan:** Conceptualization, Software. **Zhijun Yao:** Conceptualization, Investigation, Supervision, Writing – review & editing. **Jing Zhang:** Conceptualization, Investigation, Funding acquisition, Project administration, Resources, Supervision, Writing – review & editing.

Declaration of Competing Interest

The authors declare that they have no known competing financial interests or personal relationships that could have appeared to influence the work reported in this paper.

Data availability

Data will be made available on request.

Appendix A. Supplementary data

Supplementary data to this article can be found online at <https://doi.org/10.1016/j.nicl.2022.103160>.

References

- Alper, J., Seifert, A.C., Verma, G., Huang, K.H., Jacob, Y., Al Qadi, A., Rutland, J.W., Patel, S., Bederson, J., Shrivastava, R.K., Delman, B.N., Balchandani, P., 2021. Leveraging high-resolution 7-tesla MRI to derive quantitative metrics for the trigeminal nerve and subnuclei of limbic structures in trigeminal neuralgia. *J. Headache Pain* 22 (1), 112. <https://doi.org/10.1186/s10194-021-01325-4>.
- Andica, C., Kamagata, K., Hatano, T., Saito, Y., Ogaki, K., Hattori, N., Aoki, S., 2020. MR biomarkers of degenerative brain disorders derived from diffusion imaging. *J. Magn. Reson. Imaging* 52 (6), 1620–1636. <https://doi.org/10.1002/jmri.27019>.
- Antón-Bolaños, N., Espinosa, A., López-Bendito, G., 2018. Developmental interactions between thalamus and cortex: a true love reciprocal story. *Curr. Opin. Neurobiol.* 52, 33–41. <https://doi.org/10.1016/j.conb.2018.04.018>.
- Baliki, M.N., Geha, P.Y., Apkarian, A.V., Chialvo, D.R., 2008. Beyond feeling: chronic pain hurts the brain, disrupting the default-mode network dynamics. *J. Neurosci.* 28 (6), 1398–1403. <https://doi.org/10.1523/jneurosci.4123-07.2008>.
- Baum, G.L., Cui, Z., Roalf, D.R., Ciric, R., Betzel, R.F., Larsen, B., Cieslak, M., Cook, P.A., Xia, C.H., Moore, T.M., Ruparel, K., Oathes, D.J., Alexander-Bloch, A.F., Shinohara, R.T., Raznahan, A., Gur, R.E., Gur, R.C., Bassett, D.S., Satterthwaite, T.D., 2020. Development of structure-function coupling in human brain networks during youth. *Proc. Natl. Acad. Sci. U. S. A.* 117 (1), 771–778. <https://doi.org/10.1073/pnas.1912034117>.
- Bendtsen, L., Zakrzewska, J.M., Heinskou, T.B., Hodaie, M., Leal, P.R.L., Nurmikko, T., Obermann, M., Cruccu, G., Maarbjerg, S., 2020. Advances in diagnosis, classification, pathophysiology, and management of trigeminal neuralgia. *Lancet Neurol.* 19 (9), 784–796. [https://doi.org/10.1016/s1474-4422\(20\)30233-7](https://doi.org/10.1016/s1474-4422(20)30233-7).
- Bullmore, E., Sporns, O., 2009. Complex brain networks: graph theoretical analysis of structural and functional systems. *Nat. Rev. Neurosci.* 10 (3), 186–198. <https://doi.org/10.1038/nrn2575>.
- Cao, R., Wang, X., Gao, Y., Li, T., Zhang, H., Hussain, W., Xie, Y., Wang, J., Wang, B., Xiang, J., 2020. Abnormal anatomical rich-club organization and structural-functional coupling in mild cognitive impairment and Alzheimer's Disease. *Front. Neurol.* 11, 53. <https://doi.org/10.3389/fneur.2020.00053>.
- Chao-Gan, Y., Yu-Feng, Z., 2010. DPARSF: A MATLAB Toolbox for “Pipeline” Data Analysis of Resting-State fMRI. *Front. Syst. Neurosci.* 4, 13. <https://doi.org/10.3389/fnsys.2010.00013>.
- Chiapparini, L., Ferraro, S., Grazzi, L., Bussone, G., 2010. Neuroimaging in chronic migraine. *Neurol. Sci.* 31 (Suppl 1), S19–S22. <https://doi.org/10.1007/s10072-010-0266-9>.
- Headache Classification Committee, 2018. Headache Classification Committee of the International Headache Society (IHS) The International Classification of Headache Disorders, 3rd edition. *Cephalalgia* 38 (1), 1–211. <https://doi.org/10.1177/0333102417738202>.
- Crossley, N.A., Mechelli, A., Vértes, P.E., Winton-Brown, T.T., Patel, A.X., Ginestet, C.E., McGuire, P., Bullmore, E.T., 2013. Cognitive relevance of the community structure of the human brain functional coactivation network. *Proc. Natl. Acad. Sci. U. S. A.* 110 (28), 11583–11588. <https://doi.org/10.1073/pnas.1220826110>.
- Cruccu, G., Di Stefano, G., Truini, A., 2020. Trigeminal neuralgia. *N. Engl. J. Med.* 383 (8), 754–762. <https://doi.org/10.1056/NEJMra1914484>.
- Cui, Z., Zhong, S., Xu, P., He, Y., Gong, G., 2013. PANDA: a pipeline toolbox for analyzing brain diffusion images. *Front. Hum. Neurosci.* 7, 42. <https://doi.org/10.3389/fnhum.2013.00042>.
- Dai, Z., Lin, Q., Li, T., Wang, X., Yuan, H., Yu, X., He, Y., Wang, H., 2019. Disrupted structural and functional brain networks in Alzheimer's disease. *Neurobiol. Aging* 75, 71–82. <https://doi.org/10.1016/j.neurobiolaging.2018.11.005>.
- Danyluk, H., Lee, E.K., Wong, S., Sajida, S., Broad, R., Wheatley, M., Elliott, C., Sankar, T., 2020. Hippocampal and trigeminal nerve volume predict outcome of surgical treatment for trigeminal neuralgia. *Cephalalgia* 40 (6), 586–596. <https://doi.org/10.1177/0333102419877659>.
- Danyluk, H., Lang, S., Monchi, O., Sankar, T., 2021. Pre-operative limbic system functional connectivity distinguishes responders from non-responders to surgical treatment for trigeminal neuralgia. *Front. Neurol.* 12, 716500. <https://doi.org/10.3389/fneur.2021.716500>.
- Davis, K.D., Taylor, K.S., Anastakis, D.J., 2011. Nerve injury triggers changes in the brain. *Neuroscientist* 17 (4), 407–422. <https://doi.org/10.1177/1073858410389185>.
- De Pauw, R., Aerts, H., Siugzdaitė, R., Meeus, M., Coppieters, I., Caeyenberghs, K., Cagnie, B., 2020. Hub disruption in patients with chronic neck pain: a graph analytical approach. *Pain* 161 (4), 729–741. <https://doi.org/10.1097/j.pain.0000000000001762>.
- DeSouza, D.D., Hodaie, M., Davis, K.D., 2014. Abnormal trigeminal nerve microstructure and brain white matter in idiopathic trigeminal neuralgia. *Pain* 155 (1), 37–44. <https://doi.org/10.1016/j.pain.2013.08.029>.
- DeSouza, D.D., Davis, K.D., Hodaie, M., 2015. Reversal of insular and microstructural nerve abnormalities following effective surgical treatment for trigeminal neuralgia. *Pain* 156 (6), 1112–1123. <https://doi.org/10.1097/j.pain.0000000000000156>.
- Fan, L., Li, H., Zhuo, J., Zhang, Y., Wang, J., Chen, L., Yang, Z., Chu, C., Xie, S., Laird, A. R., Fox, P.T., Eickhoff, S.B., Yu, C., Jiang, T., 2016. The Human Brainnetome Atlas: A New Brain Atlas Based on Connectome Architecture. *Cereb. Cortex* 26 (8), 3508–3526. <https://doi.org/10.1093/cercor/bhw157>.
- Gong, G., Rosa-Neto, P., Carbonell, F., Chen, Z.J., He, Y., Evans, A.C., 2009. Age- and gender-related differences in the cortical anatomical network. *J. Neurosci.* 29 (50), 15684–15693. <https://doi.org/10.1523/jneurosci.2308-09.2009>.
- Guo, X., Yang, F., Fan, L., Gu, Y., Ma, J., Zhang, J., Liao, M., Zhai, T., Zhang, Y., Li, L., Su, L., Dai, Z., 2021. Disruption of functional and structural networks in first-episode, drug-naïve adolescents with generalized anxiety disorder. *J. Affect. Disord.* 284, 229–237. <https://doi.org/10.1016/j.jad.2021.01.088>.
- Hagmann, P., Cammoun, L., Gigandet, X., Meuli, R., Honey, C.J., Wedeen, V.J., Sporns, O., Friston, K.J., 2008. Mapping the structural core of human cerebral cortex. *PLoS Biol.* 6 (7), e159.
- Hagmann, P., Sporns, O., Madan, N., Cammoun, L., Pienaar, R., Wedeen, V.J., Meuli, R., Thiran, J.P., Grant, P.E., 2010. White matter maturation reshapes structural connectivity in the late developing human brain. *Proc. Natl. Acad. Sci. U. S. A.* 107 (44), 19067–19072. <https://doi.org/10.1073/pnas.1009073107>.
- Harris, H.N., Peng, Y.B., 2020. Evidence and explanation for the involvement of the nucleus accumbens in pain processing. *Neural Regen Res.* 15 (4), 597–605. <https://doi.org/10.4103/1673-5374.266909>.
- Henssen, D., Dijk, J., Kneplé, R., Sieffers, M., Winter, A., Vissers, K., 2019a. Alterations in grey matter density and functional connectivity in trigeminal neuropathic pain and trigeminal neuralgia: A systematic review and meta-analysis. *Neuroimage Clin.* 24, 102039. <https://doi.org/10.1016/j.nicl.2019.102039>.
- Henssen, D., Dijk, J., Kneplé, R., Sieffers, M., Winter, A., Vissers, K., 2019b. Alterations in grey matter density and functional connectivity in trigeminal neuropathic pain and trigeminal neuralgia: A systematic review and meta-analysis. *Neuroimage Clin.* 24, 102039. <https://doi.org/10.1016/j.nicl.2019.102039>.
- Henssen, D.J.H.A., Hoefsloot, W., Groenen, P.S.M., Van Cappellen van Walsum, A.M., Kurt, E., Kozicz, T., van Dongen, R., Schutter, D.J.L.G., Bartels, R.H.M.A., 2019c. Bilateral vs. unilateral repetitive transcranial magnetic stimulation to treat neuropathic orofacial pain: A pilot study. *Brain Stimulation* 12 (3), 803–805.
- Holste, K., Chan, A.Y., Rolston, J.D., Englot, D.J., 2020. Pain outcomes following microvascular decompression for drug-resistant trigeminal neuralgia: A systematic review and meta-analysis. *Neurosurgery* 86 (2), 182–190. <https://doi.org/10.1093/neuros/nyz075>.
- Honey, C.J., Sporns, O., Cammoun, L., Gigandet, X., Thiran, J.P., Meuli, R., Hagmann, P., 2009. Predicting human resting-state functional connectivity from structural connectivity. *Proc. Natl. Acad. Sci. U. S. A.* 106 (6), 2035–2040. <https://doi.org/10.1073/pnas.0811168106>.
- Islam, J., Kc, E., Kim, S., Kim, H.K., Park, Y.S., 2021. Stimulating GABAergic neurons in the nucleus accumbens core alters the trigeminal neuropathic pain responses in a rat model of infraorbital nerve injury. *Int. J. Mol. Sci.* 22 (16). <https://doi.org/10.3390/ijms22168421>.
- Iwata, K., Kamo, H., Ogawa, A., Tsuboi, Y., Noma, N., Mitsuhashi, Y., Taira, M., Koshikawa, N., Kitagawa, J., 2005. Anterior cingulate cortical neuronal activity during perception of noxious thermal stimuli in monkeys. *J. Neurophysiol.* 94 (3), 1980–1991. <https://doi.org/10.1152/jn.00190.2005>.
- Kaplan, C.M., Schrepf, A., Vatansever, D., Larkin, T.E., Mawla, I., Ichesco, E., Kochlefl, L., Harte, S.E., Clauw, D.J., Mashour, G.A., Harris, R.E., 2019. Functional and neurochemical disruptions of brain hub topology in chronic pain. *Pain* 160 (4), 973–983. <https://doi.org/10.1097/j.pain.0000000000001480>.
- Kim, D.J., Min, B.K., 2020. Rich-club in the brain's macrostructure: Insights from graph theoretical analysis. *Comput. Struct. Biotechnol. J.* 18, 1761–1773. <https://doi.org/10.1016/j.csbj.2020.06.039>.
- Klein, M.M., Treister, R., Raji, T., Pascual-Leone, A., Park, L., Nurmikko, T., Lenz, F., Lefaucheur, J.P., Lang, M., Hallett, M., Fox, M., Cudkovic, M., Costello, A., Carr, D. B., Ayache, S.S., Oaklander, A.L., 2015. Transcranial magnetic stimulation of the brain: guidelines for pain treatment research. *Pain* 156 (9), 1601–1614. <https://doi.org/10.1097/j.pain.0000000000000210>.
- Kumar, V.J., van Oort, E., Scheffler, K., Beckmann, C.F., Grodd, W., 2017. Functional anatomy of the human thalamus at rest. *Neuroimage* 147, 678–691. <https://doi.org/10.1016/j.neuroimage.2016.12.071>.
- Li, K., Liu, L., Yin, Q., Dun, W., Xu, X., Liu, J., Zhang, M., 2017. Abnormal rich club organization and impaired correlation between structural and functional connectivity in migraine sufferers. *Brain Imaging Behav.* 11 (2), 526–540. <https://doi.org/10.1007/s11682-016-9533-6>.
- Liu, S., Wang, S., Zhang, M., Xu, Y., Shao, Z., Chen, L., Yang, W., Liu, J., Yuan, K., 2021. Brain responses to drug cues predict craving changes in abstinent heroin users: A preliminary study. *Neuroimage* 237, 118169. <https://doi.org/10.1016/j.neuroimage.2021.118169>.
- Liu, J., Zhao, L., Lei, F., Zhang, Y., Yuan, K., Gong, Q., Liang, F., Tian, J., 2015. Disrupted resting-state functional connectivity and its changing trend in migraine sufferers. *Hum. Brain Mapp.* 36 (5), 1892–1907. <https://doi.org/10.1002/hbm.22744>.
- Liu, J., Zhu, J., Yuan, F., Zhang, X., Zhang, Q., 2018. Abnormal brain white matter in patients with right trigeminal neuralgia: a diffusion tensor imaging study. *J. Headache Pain* 19 (1), 46. <https://doi.org/10.1186/s10194-018-0871-1>.
- Mansour, A.R., Baliki, M.N., Huang, L., Torbey, S., Herrmann, K.M., Schnitzer, T.J., Apkarian, V.A., 2013. Brain white matter structural properties predict transition to chronic pain. *Pain* 154 (10), 2160–2168. <https://doi.org/10.1016/j.pain.2013.06.044>.
- May, A., 2008. Chronic pain may change the structure of the brain. *Pain* 137 (1), 7–15. <https://doi.org/10.1016/j.pain.2008.02.034>.
- Mišić, B., Betzel, R.F., de Reus, M.A., van den Heuvel, M.P., Berman, M.G., McIntosh, A. R., Sporns, O., 2016. Network-level structure-function relationships in human neocortex. *Cereb. Cortex* 26 (7), 3285–3296. <https://doi.org/10.1093/cercor/bhw089>.
- Mori, S., Crain, B.J., Chacko, V.P., van Zijl, P.C., 1999. Three-dimensional tracking of axonal projections in the brain by magnetic resonance imaging. *Ann. Neurol.* 45 (2), 265–269. [https://doi.org/10.1002/1531-8249\(199902\)45:2<265::aid-ana21>3.0.co;2-3](https://doi.org/10.1002/1531-8249(199902)45:2<265::aid-ana21>3.0.co;2-3).
- Mueller, D., Obermann, M., Yoon, M.S., Poitz, F., Hansen, N., Slomke, M.A., Dommès, P., Gizewski, E., Diener, H.C., Katsarava, Z., 2011. Prevalence of trigeminal neuralgia

- and persistent idiopathic facial pain: a population-based study. *Cephalalgia* 31 (15), 1542–1548. <https://doi.org/10.1177/0333102411424619>.
- Neudorf, J., Ekstrand, C., Kress, S., Borowsky, R., 2020. Brain structural connectivity predicts brain functional complexity: diffusion tensor imaging derived centrality accounts for variance in fractal properties of functional magnetic resonance imaging signal. *Neuroscience* 438, 1–8. <https://doi.org/10.1016/j.neuroscience.2020.04.048>.
- Noorani, A., Hung, P.S., Zhang, J.Y., Sohng, K., Laperriere, N., Moayed, M., Hodaie, M., 2022. Pain relief reverses hippocampal abnormalities in trigeminal neuralgia. *J. Pain* 23 (1), 141–155. <https://doi.org/10.1016/j.jpain.2021.07.004>.
- Peng, Z., Yang, X., Xu, C., Wu, X., Yang, Q., Wei, Z., Zhou, Z., Verguts, T., Chen, Q., 2021. Aberrant rich club organization in patients with obsessive-compulsive disorder and their unaffected first-degree relatives. *Neuroimage Clin.* 32, 102808 <https://doi.org/10.1016/j.nicl.2021.102808>.
- Petrovic, P., Ingvar, M., 2002. Imaging cognitive modulation of pain processing. *Pain* 95 (1–2), 1–5. [https://doi.org/10.1016/s0304-3959\(01\)00467-5](https://doi.org/10.1016/s0304-3959(01)00467-5).
- Peyron, R., Laurent, B., Garcia-Larrea, L., 2000. Functional imaging of brain responses to pain. A review and meta-analysis (2000). *Neurophysiologie Clinique/Clinical Neurophysiology* 30 (5), 263–288.
- Porcaro, C., Di Renzo, A., Tinelli, E., Di Lorenzo, G., Parisi, V., Caramia, F., Fiorelli, M., Di Piero, V., Pierelli, F., Coppola, G., 2020. Haemodynamic activity characterization of resting state networks by fractal analysis and thalamocortical morphofunctional integrity in chronic migraine. *J. Headache Pain* 21 (1), 112. <https://doi.org/10.1186/s10194-020-01181-8>.
- Price, D.D., 2002. Central neural mechanisms that interrelate sensory and affective dimensions of pain. *Mol. Interv.* 2 (6), 392–403.
- Robison, A.J., Nestler, E.J., 2011. Transcriptional and epigenetic mechanisms of addiction. *Nat. Rev. Neurosci.* 12 (11), 623–637. <https://doi.org/10.1038/nrn3111>.
- Rubinov, M., Sporns, O., 2010. Complex network measures of brain connectivity: uses and interpretations. *Neuroimage* 52 (3), 1059–1069. <https://doi.org/10.1016/j.neuroimage.2009.10.003>.
- Sabalys, G., Juodzbalys, G., Wang, H.L., 2013. Aetiology and pathogenesis of trigeminal neuralgia: a comprehensive review. *J. Oral Maxillofac. Res.* 3 (4), e2.
- Seminowicz, D.A., Mikulis, D.J., Davis, K.D., 2004. Cognitive modulation of pain-related brain responses depends on behavioral strategy. *Pain* 112 (1–2), 48–58. <https://doi.org/10.1016/j.pain.2004.07.027>.
- Shu, N., Wang, X., Bi, Q., Zhao, T., Han, Y., 2018. Disrupted topologic efficiency of white matter structural connectome in individuals with subjective cognitive decline. *Radiology* 286 (1), 229–238. <https://doi.org/10.1148/radiol.2017162696>.
- Smith, S.M., Jenkinson, M., Woolrich, M.W., Beckmann, C.F., Behrens, T.E., Johansen-Berg, H., Bannister, P.R., De Luca, M., Drobnjak, I., Flitney, D.E., Niaz, R.K., Saunders, J., Vickers, J., Zhang, Y., De Stefano, N., Brady, J.M., Matthews, P.M., 2004. Advances in functional and structural MR image analysis and implementation as FSL. *Neuroimage* 23 (Suppl 1), S208–S219. <https://doi.org/10.1016/j.neuroimage.2004.07.051>.
- Stam, C.J., 2014. Modern network science of neurological disorders. *Nat. Rev. Neurosci.* 15 (10), 683–695. <https://doi.org/10.1038/nrn3801>.
- Supekar, K., Uddin, L.Q., Prater, K., Amin, H., Greicius, M.D., Menon, V., 2010. Development of functional and structural connectivity within the default mode network in young children. *Neuroimage* 52 (1), 290–301. <https://doi.org/10.1016/j.neuroimage.2010.04.009>.
- Taylor, K.S., Anastakis, D.J., Davis, K.D., 2009. Cutting your nerve changes your brain. *Brain* 132 (Pt 11), 3122–3133. <https://doi.org/10.1093/brain/awp231>.
- Tian, T., Guo, L., Xu, J., Zhang, S., Shi, J., Liu, C., Qin, Y., Zhu, W., 2016. Brain white matter plasticity and functional reorganization underlying the central pathogenesis of trigeminal neuralgia. *Sci. Rep.* 6, 36030. <https://doi.org/10.1038/srep36030>.
- Tsai, Y.H., Yuan, R., Patel, D., Chandrasekaran, S., Weng, H.H., Yang, J.T., Lin, C.P., Biswal, B.B., 2018. Altered structure and functional connection in patients with classical trigeminal neuralgia. *Hum. Brain Mapp.* 39 (2), 609–621. <https://doi.org/10.1002/hbm.23696>.
- Tsai, Y.H., Liang, X., Yang, J.T., Hsu, L.M., 2019. Modular organization of brain resting state networks in patients with classical trigeminal neuralgia. *Neuroimage Clin.* 24, 102027 <https://doi.org/10.1016/j.nicl.2019.102027>.
- Tsubokawa, T., Katayama, Y., Yamamoto, T., Hirayama, T., Koyama, S., 1991. Chronic motor cortex stimulation for the treatment of central pain. *Acta Neurochir. Suppl. (Wien.)* 52, 137–139. https://doi.org/10.1007/978-3-7091-9160-6_37.
- Tu, Y., Jung, M., Gollub, R.L., Napadow, V., Gerber, J., Ortiz, A., Lang, C., Mawla, I., Shen, W., Chan, S.T., Wasan, A.D., Edwards, R.R., Kaptchuk, T.J., Rosen, B., Kong, J., 2019. Abnormal medial prefrontal cortex functional connectivity and its association with clinical symptoms in chronic low back pain. *Pain* 160 (6), 1308–1318. <https://doi.org/10.1097/j.pain.0000000000001507>.
- van den Heuvel, M.P., Kahn, R.S., Goñi, J., Sporns, O., 2012. High-cost, high-capacity backbone for global brain communication. *Proc. Natl. Acad. Sci. U. S. A.* 109 (28), 11372–11377. <https://doi.org/10.1073/pnas.1203593109>.
- van den Heuvel, M.P., Sporns, O., 2011. Rich-club organization of the human connectome. *J. Neurosci.* 31 (44), 15775–15786. <https://doi.org/10.1523/jneurosci.3539-11.2011>.
- van den Heuvel, M.P., Sporns, O., Collin, G., Scheewe, T., Mandl, R.C., Cahn, W., Goñi, J., Hulshoff Pol, H.E., Kahn, R.S., 2013. Abnormal rich club organization and functional brain dynamics in schizophrenia. *JAMA Psychiatry* 70 (8), 783–792. <https://doi.org/10.1001/jamapsychiatry.2013.1328>.
- Wang, R., Benner, T., Sorensen, A., Wedeen, V.J., 2007. Diffusion toolkit: A software package for diffusion imaging data processing and tractography. *Proc. Intl. Soc. Mag. Reson. Med.* 15.
- Wang, Y., Cao, D.Y., Remeniuk, B., Krimmel, S., Seminowicz, D.A., Zhang, M., 2017. Altered brain structure and function associated with sensory and affective components of classic trigeminal neuralgia. *Pain* 158 (8), 1561–1570. <https://doi.org/10.1097/j.pain.0000000000000951>.
- Wang, X., Qin, J., Zhu, J., Bi, K., Zhang, S., Yan, R., Zhao, P., Yao, Z., Lu, Q., 2019. Rehabilitative compensatory mechanism of hierarchical subnetworks in major depressive disorder: A longitudinal study across multi-sites. *Eur. Psychiatry* 58, 54–62. <https://doi.org/10.1016/j.eurpsy.2019.02.004>.
- Wang, J., Wang, L., Zang, Y., Yang, H., Tang, H., Gong, Q., Chen, Z., Zhu, C., He, Y., 2009. Parcellation-dependent small-world brain functional networks: a resting-state fMRI study. *Hum. Brain Mapp.* 30 (5), 1511–1523. <https://doi.org/10.1002/hbm.20623>.
- Wang, J., Wang, X., Xia, M., Liao, X., Evans, A., He, Y., 2015. GREYNET: a graph theoretical network analysis toolbox for imaging connectomics. *Front. Hum. Neurosci.* 9, 386. <https://doi.org/10.3389/fnhum.2015.00386>.
- Wu, M., Jiang, X., Qiu, J., Fu, X., Niu, C., 2020. Gray and white matter abnormalities in primary trigeminal neuralgia with and without neurovascular compression. *J. Headache Pain* 21 (1), 136. <https://doi.org/10.1186/s10194-020-01205-3>.
- Xia, M., Wang, J., He, Y., Csermely, P., 2013. BrainNet Viewer: a network visualization tool for human brain connectomics. *PLoS One* 8 (7), e68910.
- Yan, T., Wang, W., Yang, L., Chen, K., Chen, R., Han, Y., 2018. Rich club disturbances of the human connectome from subjective cognitive decline to Alzheimer's disease. *Theranostics* 8 (12), 3237–3255. <https://doi.org/10.7150/thno.23772>.
- Yeo, B.T., Krienen, F.M., Sepulcre, J., Sabuncu, M.R., Lashkari, D., Hollinshead, M., Roffman, J.L., Smoller, J.W., Zöllei, L., Polimeni, J.R., Fischl, B., Liu, H., Buckner, R. L., 2011. The organization of the human cerebral cortex estimated by intrinsic functional connectivity. *J. Neurophysiol.* 106 (3), 1125–1165. <https://doi.org/10.1152/jn.00338.2011>.
- Yu, R., Gollub, R.L., Spaeth, R., Napadow, V., Wasan, A., Kong, J., 2014. Disrupted functional connectivity of the periaqueductal gray in chronic low back pain. *Neuroimage Clin.* 6, 100–108. <https://doi.org/10.1016/j.nicl.2014.08.019>.
- Zakrzewska, J.M., Akram, H., 2011. Neurosurgical interventions for the treatment of classical trigeminal neuralgia. *Cochrane Database Syst. Rev.* 9, Cd007312. <https://doi.org/10.1002/14651858.CD007312.pub2>.
- Zalesky, A., Fornito, A., Bullmore, E.T., 2010. Network-based statistic: identifying differences in brain networks. *Neuroimage* 53 (4), 1197–1207. <https://doi.org/10.1016/j.neuroimage.2010.06.041>.
- Zhang, P., Jiang, Y., Liu, G., Han, J., Wang, J., Ma, L., Hu, W., Zhang, J., 2021. Altered brain functional network dynamics in classic trigeminal neuralgia: a resting-state functional magnetic resonance imaging study. *J. Headache Pain* 22 (1), 147. <https://doi.org/10.1186/s10194-021-01354-z>.
- Zhang, Z., Liao, W., Chen, H., Mantini, D., Ding, J.R., Xu, Q., Wang, Z., Yuan, C., Chen, G., Jiao, Q., Lu, G., 2011. Altered functional-structural coupling of large-scale brain networks in idiopathic generalized epilepsy. *Brain* 134 (Pt 10), 2912–2928. <https://doi.org/10.1093/brain/awr223>.